Sub-graph entropy based network approaches for classifying adolescent obsessive-compulsive disorder from resting-state functional MRI

Bhaskar Sen[a], Gail A. Bernstein[b], Bryon A. Mueller[b], Kathryn R. Cullen[b], Keshab K. Parhi[*,a]

[a] Department of Electrical and Computer Engineering, University of Minnesota, Minneapolis
[b] Department of Psychiatry & Behavioral Sciences, University of Minnesota, Minneapolis

ARTICLE INFO

Keywords:
Sub-graph entropy
Functional network
Obsessive compulsive disorder
Classification
Psychiatry

ABSTRACT

This paper presents a novel approach for classifying obsessive-compulsive disorder (OCD) in adolescents from resting-state fMRI data. Currently, the state-of-the-art for diagnosing OCD in youth involves interviews with adolescent patients and their parents by an experienced clinician, symptom rating scales based on Diagnostic and Statistical Manual of Mental Disorders (DSM), and behavioral observation. Discovering signal processing and network-based biomarkers from functional magnetic resonance imaging (fMRI) scans of patients has the potential to assist clinicians in their diagnostic assessments of adolescents suffering from OCD. This paper investigates the clinical diagnostic utility of a set of *univariate, bivariate* and *multivariate* features extracted from resting-state fMRI using an *information-theoretic* approach in 15 adolescents with OCD and 13 matched healthy controls. Results indicate that an *information-theoretic* approach based on *sub-graph* entropy is capable of classifying OCD *vs.* healthy subjects with high accuracy. Mean time-series were extracted from 85 brain regions and were used to calculate Shannon wavelet entropy, Pearson correlation matrix, network features and *sub-graph* entropy. In addition, two special cases of *sub-graph* entropy, namely node and edge entropy, were investigated to identify important brain regions and edges from OCD patients. A leave-one-out cross-validation method was used for the final predictor performance. The proposed methodology using *differential sub-graph* (edge) entropy achieved an accuracy of 0.89 with specificity 1 and sensitivity 0.80 using leave-one-out cross-validation with in-fold feature ranking and selection. The high classification accuracy indicates the predictive power of the sub-network as well as edge entropy metric.

1. Introduction

Obsessive-compulsive disorder (OCD) is a serious psychiatric illness that affects about 2 - 3% of the population worldwide (Rasmussen and Eisen, 1992). Onset of OCD is associated with excessive intrusive, unwanted thoughts (obsessions) and repetitive behaviors (compulsions). This paper addresses discriminating and classifying the brain state of adolescents with OCD from healthy controls using resting-state functional magnetic resonance imaging (fMRI). Identifying features for discriminating OCD in adolescents is an important topic of research that could lead to useful clinical tools to aid in the diagnosis and management of youth with OCD. The current psychiatric diagnostic practices for adolescents include interviews with youths and their parents by experienced clinicians, symptom rating scales and behavioral examinations (Grabill et al., 2008; King et al., 1998). However, there are no evidence-based neurobiological markers available to aid clinicians in the diagnosis. Finding the brain regions and functional

connections that are affected during OCD among adolescents is still an active area of research.

Past research has shown that fMRI is a useful tool for understanding psychiatric disorders (Bassett et al., 2012; Mitterschiffthaler et al., 2006). Broadly, fMRI provides a non-invasive way to measure activity of the brain during resting-state (rs-fMRI) or task (t-fMRI) using the change of blood-oxygen level dependent (BOLD) signal (Sen and Parhi, 2017). The fMRI scans of a person can be used to generate the functional connectivity network of the brain. In particular, rs-fMRI measures the spontaneous fluctuation of BOLD signal during awake rest. In case of many psychiatric diseases, the rs-fMRI signal is highly meaningful as it is not confounded by any task-based performance (Dragomir et al., 2018; Greicius et al., 2003). The rs-fMRI signal from a given brain region can yield particular properties of neurobiological interest such as amplitude and signal entropy (Bassett et al., 2012). In this paper, we are only concerned about the rs-fMRI analysis for adolescents with OCD and healthy

---

Table 1

Demographic and clinical characteristics of the OCD and control groups. CY-BOCS: children's yale-brown obsessive compulsive scale (Bernstein et al., 2013; Rosario-Campos et al., 2006) .

Demographic information	OCD	Control	t or χ^2	p-value
# of samples (n)	15	13	–	–
Age at onset - mean (SD)	9.5 (4.0)	–	–	–
Age at assessment - mean(SD, maximum, minimum)	15.3 (2.1, 19, 12.3)	16 (1.8, 18.8, 12.3)	$t = 0.98$	0.34
Male n(%)	8 (53)	7 (54)	$\chi^2 = 0.001$	0.98
Clinical Information - CY-BOCS	OCD	Control	t or χ^2	p-value
Obsessions, mean (SD)	9.4 (2.2)	0.1(0.3)	$t = 15.9$	< 0.001
Compulsions, mean (SD)	10.3 (1.7)	0.0 (0.0)	$t = 22.1$	< 0.001
Total, mean (SD, maximum, minimum)	19.7 (3.5, 27, 12)	0.1 (0.3)	$t = 19.9$	< 0.001

controls.

The human brain is a network of interconnected nodes or regions functionally connected with each other (Atluri et al., 2016). Each regional brain activity is described by a time-series that is calculated by averaging all the time-series corresponding to the voxels for that region and the functional connection is measured by correlation coefficients between the regions (Bullmore and Sporns, 2009; Sporns, 2003). Recent advancements in neuroimaging and network theory offer tools that may be useful to advance understanding of psychiatric illnesses such as OCD. For example, entropy is a concept with origins in physics but more recently adopted by information theory and indexes unpredictability and complexity. A univariate measure of entropy can be calculated from any time-series data from a particular brain region. A multivariate measure of entropy can also be calculated to describe the complexity of a graph. We recently introduced the approach of examining entropy of *sub-graphs* which was capable of classifying brain states with high accuracy (Sen et al., 2019). Furthermore, *sub-graph entropy* can be used to rank regions and edges within a brain network with respect to their differential values between two groups, and the ranking carries useful information about the disruption in brain network due to a disorder.

The goal of this study was to apply advanced rs-fMRI analytical approaches for analyzing rs-fMRI data to classify adolescents with OCD *vs.* healthy controls. We used time-series, absolute correlation coefficients and graph-theoretic properties of functional network for these classifications. Although many brain network statistics exist in the literature and have been used to rank regions (nodes) or functional connections (edges), the proposed approach has never been applied to brain networks for diagnosing psychiatric disorders. First we used *univariate* (*e.g.*, Shannon wavelet entropy of each time-series), *bivariate* (absolute value of Pearson correlation) and *multivariate* (network features, *e.g., local efficiency, global efficiency* (Latora and Marchiori, 2001; Sporns, 2003), *clustering coefficient* (Rubinov and Sporns, 2010), *betweenness centrality* (Freeman et al., 1979), *modularity* (Newman, 2006), graph and *sub-graph* entropy (Sen et al., 2019)) features for predicting OCD. These measures describe *segregation* or *integration* within the network. Next, network measures such as *sub-graph* entropy (Sen et al., 2019) and specifically those of nodes and edges were used to rank important brain regions and edges in each group of brain networks. In addition, the nodes and edges were also ranked by the extent to which they differentiated groups. This led to extracting a sub-network containing 120 edges, which was used for classification of OCD *vs.* controls.

Some of the above network measures have been used previously for comparing characteristics between two groups (e.g., schizophrenia *vs.* healthy (Bassett et al., 2012; Huang et al., 2018), Alzheimer's disorder *vs.* healthy (Armañanzas et al., 2016; Dragomir et al., 2018), borderline personality disorder *vs.* healthy (Xu et al., 2016), and obsessive-compulsive disorder *vs.* healthy (Armstrong et al., 2016)). While these traditional association studies can extract statistically significant neural correlates for a disorder, in this paper we extract a sub-network from resting-state fMRI data from two groups of adolescents that can predict whether a subject has OCD.

2. Materials and methods

2.1. Dataset and preprocessing

We describe the dataset and the preprocessing steps following the procedure outlined in Bernstein et al. (2016). Fifteen adolescents with OCD and 13 matched healthy control subjects were enrolled for the study. There were no significant differences between the OCD and control groups in terms of age, gender, socioeconomic status, IQ, ethnicity and handedness (Bernstein et al., 2016). Children's Yale-Brown Obsessive-Compulsive Scale (CY-BOCS) checklist (Rosario-Campos et al., 2006) was used to calculate scores on 4 factor-analyzed symptom dimension (Bernstein et al., 2013). OCD patients had mean Y-BOCS score of 19.7 (standard deviation SD = 3.5, max 27, min 12) whereas the healthy controls had mean Y-BOCS score 0.1 (SD 0.3). Mean age for onset of the disease is 9.5 ± 4.0 years. The mean duration of the patients for the disease is 5.8 ± 4.2 years. Twelve out of 15 OCD subjects were on psychotropic medication. Details about age at assessment and clinical information for the adolescent are given in Table 1. More specifically, the mean age at the assessment for OCD subjects and controls were 15.3 (maximum 19, minimum 12.3) and 16 (max 18.8, min 12.3), respectively. Number of males in the groups were 8 and 7 for OCD and control groups, respectively. Resting-state fMRI scans (2 sessions each of 12 minutes duration) were taken using a novel multiband EPI sequence that accounts for acquiring multiple slices simultaneously (Feinberg et al., 2010). The rs-fMRI scans were acquired with the following parameters TR = 1.15 s, TE = 30 ms, voxel size = 2 mm isotropic, 60 slices, multiband factor = 4, echo spacing = 0.57 ms and number of 3D volumes = 600. During the scans, the subjects were asked to remain awake, eyes closed and not to think about anything in particular. More details about the data can be found in Bernstein et al. (2016). The experimental procedures involving human subjects described in this paper were approved by the University of Minnesota *Institutional Review Board*.

FSL tool (Jenkinson et al., 2012) was used for the pre-processing of the fMRI data. The steps included skull removal, distortion correction, motion correction and registration to Montreal Neurological Institute space (**MNI**). Using FSL program **melodic**, we analyzed the independent components and those corresponding to artifacts (heart rate, respiration, movement, white matter or cerebrospinal fluid) were removed. More details of the preprocessing can be found in Bernstein et al. (2016). After the preprocessing step, Desikan atlas (Desikan et al., 2006) was used to extract mean time-series for each of the 85 cortical and sub-cortical regions available in the atlas. The list of the regions used for the analysis is given in Supplementary Information Table A1. Each time-series was then filtered by a band-pass filter with pass-band between 0.01 Hz - 0.15 Hz, followed by a decomposition into two frequency bands using a db-4 wavelet filter: lower (B1: 0.01–0.08 Hz) and higher (B2: 0.08-0.15 Hz) (Xu et al., 2016).

2.2. Univariate features

The complexity of rs-fMRI time-series was first investigated by using a *univariate* approach following Bassett et al. (2012). Here we estimated the complexity of mean time-series extracted from each brain region through Shannon wavelet entropy (Rosso et al., 2001). We only focused our investigation of two frequency bands described above. Lower frequency band oscillations of BOLD signal have been shown previously to be adversely affected during a psychiatric disease *state*, (Lynall et al., 2010). The Shannon wavelet entropy was estimated using techniques developed in Coifman and Wickerhauser (1992) and Donoho et al. (1994) and implemented in the MATLAB Wavelet Toolbox (function wentropy.m). In short, the Shannon wavelet entropy is defined as:

$$E(s) = -\sum_i s_i^2 \log(s_i^2)$$

Here s is the mean time-series of a brain region for an individual, and s_i's are the coefficients of s in the orthonormal wavelet basis.

2.3. Bivariate features

Pearson correlation coefficient ($P_{i,j}^f$) was calculated for each frequency band and the regions (r_i and r_j) where $i, j \in \{1, .85\}$ as described in Sen et al. (2016). Let r_i^f be the mean time-series from frequency band f and region i from fMRI. Then, the Pearson correlation coefficient between two regions i, j is calculated by

$$P_{i,j}^f = P_{j,i}^f = \frac{E[(r_i^f - \hat{r}_i^f)(r_j^f - \hat{r}_j^f)]}{\sqrt{E[(r_i^f - \hat{r}_i^f)^2]}\sqrt{E[(r_j^f - \hat{r}_j^f)^2]}} \tag{1}$$

where $\hat{r}_i^f$ is the estimated mean of the time-series from frequency band f and region i. Thus two adjacency matrices were created for each pair of regions corresponding to two frequency bands. These matrices can also be seen as edges in a graph where each node corresponds to one region. The total number of features for each frequency band was $\frac{85 \times 84}{2} = 3570$. Absolute values of Pearson correlations were used as features.

2.4. Multivariate features

For each subject, two 85 × 85 adjacency matrices (Sen et al., 2016) containing absolute Pearson correlation were extracted. Suppose that a group of N brain networks from R regions and N subjects is specified by the adjacency matrix $C_{R \times R}^k$ where $k \in \{1, N\}$. $R \times R$ is the size of the adjacency matrix. Here $C^k(i, j)$ is the connectivity between two regions (i, j) for subject k. Ideally $C_{R \times R}^k$ is a binary matrix where existence of an edge is given by 1 and non-existence is given by 0. However, connectivity matrices extracted from fMRI are correlation values which are non-binary. In order to calculate the network features, first the matrices were *binarized* by keeping {5%, 20%, 35%, 50%} of the edges. The sparsity of the networks for all subjects remained the same for a specific density.

2.4.1. Network features

Adjacency matrices were used to calculate network characteristics using *Brain Connectivity Toolbox* (BCT). [1] At a local (node) level in the network, three features, namely *local efficiency (LE), clustering coefficient (CC)* and *betweenness centrality (BC)*, were computed (Sen et al., 2016; Xu et al., 2016). At a global level, we calculated two features: *modularity* and *global efficiency,sen2016classification*. The local and global features in the network represent complementary viewpoints of the network for *segregation* and *integration* of nodes, respectively. Hence

---

[1] https://sites.google.com/site/bctnet/ .

from each subject, we extracted 85 × 3 × 2 (for 3 features at each node) + 2 × 2 (for *modularity and global efficiency*) = 514 network features corresponding to two frequency bands.

An overview of the network based features is discussed next as described in Sen et al. (2019). *Local efficiency* is computed using the summation of inverse of the shortest paths to the neighbors of a node. This metric is used to understand how efficient a node is for transferring information between two neighboring nodes. *Clustering coefficient* is calculated by the number of triangles created around a node out of all possible triangles. *Betweenness centrality* of a node is calculated as the percentage of shortest paths that contain the node. *Modularity* metric measures how a network is sub-divided into smaller dense sub-networks with sparse inter-connections. *Global efficiency* describes the efficiency of information transfer within the whole graph. In addition, Network Based Statistics (NBS) (Zalesky et al., 2010) is used to extract important edges between two groups. NBS is a popular method for testing hypotheses about the edges in a network using *t*-test. It is used to identify connections and networks comprising the connectome associated with an experiment for a between-group difference. These network measures were also previously used for classifying OCD *vs.* healthy from fMRI data as described in Sen et al. (2016). More details of the network measures can be found in Rubinov and Sporns (2010).

2.4.2. Sub-graph entropy

We have recently shown that *sub-graph* entropy can effectively classify brain *states* for two different tasks (Sen et al., 2019). *Sub-graph* entropy captures the interaction of local neighborhood of a brain region or functional connection in an entropy formulation. Although *sub-graph* entropy of a network (G) can be computed in multiple ways (*e.g.,* see Körner, 1973; Li and Pan, 2016), the scope of this paper is restricted to only the complexity associated with the entries in the adjacency matrix for the network. Within this limit, the current model achieves remarkable accuracy for diagnosing a common psychiatric disorder. In particular the *sub-graph* entropy is defined as the number of bits required to encode the adjacency structure of the network (Freeman et al., 1979; Mackenzie, 1966). A brief description of *sub-graph* entropy (node and edge entropy) is presented next following Sen et al. (2019).

A normalized adjacency matrix from one subject is defined as

$$Q^k = \frac{C^k}{\sum_{i,j,j\neq i}^{R,R} C^k(i, j)}. \tag{2}$$

This definition normalizes the entries in the adjacency matrix so that their summation is 1. For bi-directional networks, we just normalize the upper triangular part of C^k. We also define $q_{i,j}^k = Q^k(i, j)$.

In this case, the graph entropy is calculated by (Mackenzie, 1966)

$$H(G) = -\sum_{i=1}^{R} \sum_{j=1, i\neq j}^{R} q_{i,j} \log_2(q_{i,j}). \tag{3}$$

In our work we calculated the matrix consisting of the indices $q_{i,j}$ as in Eq. (2). Graph entropy for a subset of a network was also computed and referred as *sub-graph* entropy.

Node entropy Node entropy was calculated based on the *sub-graph* containing a region and its neighbors. We defined neighbors based on the 1-hop distances from the node, *i.e., sub-graph* containing nodes that are one edge away. Experiments involving 2-hop neighbors were also carried out and results from this analysis are presented in the Supplementary Information. The entries only signifying the interaction between one region and its neighbor were kept. All the other entries are forced to be zeros. Let the node entropy of node v_i is denoted by $H^k(G_{v_i})$ for subject k, then

$$H^k(G_{v_i}) = -\sum_{m=1}^{M} q_m^k \log_2(q_m^k), \tag{4}$$

where q_m denotes the normalized edge weight for neighborhood, and M

represents the number of edges in the *sub-graph*.

After calculating node entropy for individual subjects, the node entropy from a group of N subjects can be estimated as follows.

$$H(G_{v_i}) = \frac{1}{N} \sum_{k=1}^{N} H^k(G_{v_i}) \qquad (5)$$

An algorithm for ranking important regions based on node entropy is given in Supplementary Information (SI) (Algorithm S1).

Edge entropy Suppose region i is connected to j through edge e_{ij} where $i \neq j$. Similar to node entropy, the edge neighbors were also defined based on the 1-hop distances from the edge e_{ij}. In this case, we computed the edge entropy of subject k as $H(G_{e_{ij}})$ (Sen et al., 2019),

$$H^k(G_{e_{ij}}) = - \sum_{m=1}^{M} q_m^k \log_2(q_m^k), \qquad (6)$$

where q_m denotes the normalized edge weight for neighborhood, and M is number of edges in the *sub-graph*.

After calculating edge entropy for individual subjects, the group edge entropy from an ensemble of graphs can be estimated as follows:

$$H(G_{e_{ij}}) = \frac{1}{N} \sum_{k=1}^{N} H^k(G_{e_{ij}}). \qquad (7)$$

An algorithm for ranking important edges based on node entropy is given in SI (Algorithm S2).

Differential sub-graph (node and edge) entropy

Between two groups of subjects, if the local *segregation* of brain regions change, the change in pattern can be captured using *differential entropy,sen2019ranking*. In this case, the regions or edges which have the most change in entropies between two groups are most affected due to the change in the brain *state*. Suppose, for region i, the node entropy for subjects belonging to group G_1 (where $G_1 \in$ {Healthy, OCD etc}) is given by $H_{G_1}(G_{v_i})$ and for group G_2, $H_{G_2}(G_{v_i})$. The difference between these two values would encompass *differential entropy* between two groups of subjects for region i. The change in entropy is calculated as $|H_{G_1}(G_{v_i}) - H_{G_2}(G_{v_i})|$ where $|x|$ is the absolute value of x. This metric is called *differential node entropy,sen2019ranking*. In our experiment, *differential node entropy* was calculated for each brain region and they were ranked based on *differential entropy* in decreasing value. The same argument and ranking procedure was applied to *differential edge entropy* as well. The algorithm is given in Algorithm 1. This process extracted nodes and edges that had changed the most due to the functional altercation during the disease.

2.5. Extracting predictive sub-network based on edge entropy

In order to understand if *sub-graph* entropy measures contain predictive information, we used the edge entropy values for classification between two groups of subjects. Brain network measures have been used to discriminate between two groups in a number of previous papers to understand the significance, *e.g.*, see Sen et al. (2016) and Richiardi et al. (2013). In this framework, starting with the top-ranked edge, additional edges were added to the network in an iterative manner until the classification accuracy started dropping. At each iteration, the edge entropies of the sub-network were used in a leave-one-out fashion (Bao et al., 2019) for classifying OCD *vs.* healthy controls. Leave-one-out is a common cross-validation method for alleviating overfitting in case of small sample size classification problems which is often the case in psychiatry domain (Huang et al., 2018). The classifier used in this case was support vector machine (SVM) with radial basis kernel based on testing different models where SVM resulted in a better performance. The procedure for finding the predictive *sub-network* is shown in Fig. 1.

Additionally, two more *sub-graphs* containing *union* and *intersection* of statistically different regions and edges were tested for predictive performance (Sen et al., 2019). An anatomically defined *sub-graph* containing regions from CSTC network (Bernstein et al., 2016) was also used for baseline comparison of performance. In order to address the challenge of overfitting and establish the stability of predictive sub-network, the ranking procedure was run 28 times in a leave-one-out fashion. At each iteration, ranking was performed for 27 subjects except the left out. A histogram was then plotted for finding how many times top edges are extracted in the predictive sub-network.

2.6. Statistical analysis

The *univariate, bivariate* and *multivariate* features along with node entropy and edge entropy values were compared using a 2-sided *t*-test across different groups. Their corresponding *p*-values were also calculated and shown. Furthermore, leave-one-out classification accuracy, specificity and sensitivity were calculated to validate our approach.

3. Results

3.1. Univariate analysis

The classification performance of regional features using Shannon wavelet entropy is shown in last row of Table 2. In healthy controls and OCD patients, Shannon wavelet entropy was heterogeneously distributed throughout the brain with lowest Shannon wavelet entropy found in regions of the postcentral, cuneus, superiorparietal, paracentral and the highest was found in entorhinal, hippocampus, pallidum and thalamus. The regions that have significant difference in Shannon wavelet entropy are found in caudate, putamen, paracentral, postcentral, precuneus with $p < 0.05$ for band B1 (lower frequency band). Frequency band B2 (higher frequency band) did not have any statistical difference for Shannon wavelet entropy. The regions are shown in a brain template in Supplementary Information Fig. S1.

3.2. Bivariate analysis

Using a minimum redundancy maximum relevance (mRMR) in-fold feature selection (Peng et al., 2005), 5 features that are most important according to the criterion, were selected. The selected features belong to lower frequency sub-band (B1). The classification performance by leave-one-out method was 0.71 with specificity 0.85 and sensitivity 0.60 (shown in Table 2) using the absolute Pearson correlation coefficients. The results showed that Pearson correlation between superior temporal gyrus - temporal pole was selected 26 out of 28 times during the mRMR feature selection and leave-one-out classification. Additionally, the edge weight between precuneus - precentral gyrus was selected 25 out of 28 times. The other important edge connections (absolute pearson correlation) are inferior frontal gyrus - mid frontal gyrus, pars operculum - insular cortex and inferior temporal gyrus- mid temporal gyrus (Sen et al., 2016).

3.3. Multivariate analysis

3.3.1. Network features

Following the *bivariate* experiment as described in previous section, an in-fold mRMR feature selection was employed (with 5 most significant features) using network based features extracted from the functional brain graphs containing 85 regions. The leave-one-out classification accuracy using these five features was 0.75 with 0.73 sensitivity and 0.77 specificity (Table 2). Note that, clustering coefficient of putamen (at sparsity 35%) and hub property of cingulate gyrus (at sparsity 50%) were selected in each fold by the feature selection algorithm. The features and corresponding values for different sparsity levels for two groups are shown in SI Fig. S2. The selected features belong to lower frequency sub-band (B1).

Data: Normalized adjacency matrices from two groups of fMRI-data

Result: Ranking of Regions and Edges Based on Differential Sub-graph Entropy

dEentropyRegion = $R \times 1$ Vector;

dRegionrank = $R \times 1$ Vector;

dEntropyEdge = $\frac{R(R-1)}{2} \times 1$ Vector;

dEdgerank = $\frac{R(R-1)}{2} \times 1$ Vector;

for $1 \leq i \leq R$ **do**

    Calculate $H_{G1}(G_{v_i})$ using Eq. (5);

    Calculate $H_{G2}(G_{v_i})$ using Eq. (5);

    dEentropyRegion(i) = $|H_{G1}(G_{v_i}) - H_{G2}(G_{v_i})|$;

end

for $1 \leq e_{ij} \leq \frac{R(R-1)}{2}$ **do**

    Calculate $H_{G1}(e_{ij})$ using Eq. (7);

    Calculate $H_{G2}(e_{ij})$ using Eq. (7);

    dEntropyEdge(e_{ij}) = $|H_{G1}(e_{ij}) - H_{G2}(e_{ij})|$;

end

dRegionrank = sort(dEntropyRegion) ;

dEdgerank = sort(dEntropyEdge) ;

Algorithm 1. Ranking of Regions and Edges for Two Groups.
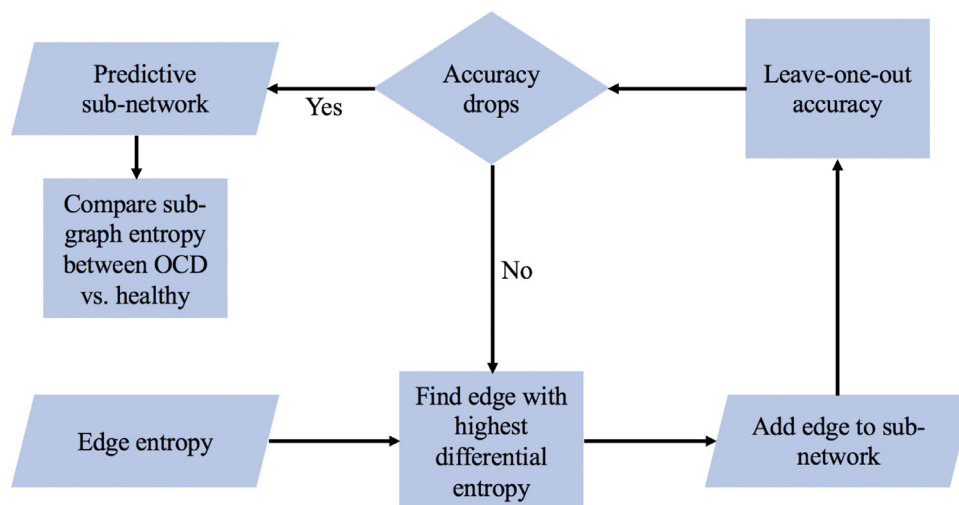
Fig. 1. Procedure for extracting a predictive sub-network for OCD *vs.* healthy. Edges with highest *differential entropy* are selected to identify the sub-network based on leave-one-out accuracy. The sub-network's *sub-graph* entropy is compared between two groups using *t*-test for validation.

Table 2
Leave-one-out classification results .

	Features	Accuracy	Specificity	Sensitivity
Proposed (edge) sub-network	120	**0.89**	**1**	**0.80**
Union sub-graph	145	**0.89**	**1**	**0.80**
Intersection sub-graph	114	0.86	0.92	0.80
CSTC sub-network	120	0.71	0.85	0.60
Node entropy (Sen et al., 2019)	85	0.71	0.62	0.80
Correlation (Sen et al., 2016)	5	0.71	0.85	0.60
Network features (Sen et al., 2016)	5	0.75	0.77	0.73
Correlation + Network features (Sen et al., 2016)	10	0.78	0.85	0.73
NBS (Zalesky et al., 2010)	95	0.64	0.54	0.73
Shannon wavelet entropy (Bassett et al., 2012)	85	0.54	0.38	0.66

3.3.2. Ranking of brain regions

The lower frequency band (B1) at network sparsity level 35% was used for calculating *sub-graph* entropy based on the classification performance. All results presented in the paper and the SI correspond to frequency band B1 and network sparsity level 35%. Using the strategy for group ranking as formulated in Eq. (5) and Algorithm S1 in Supplementary Information, we identified important regions for OCD and healthy group separately (Fig. 2). The regions identified among the top-25 in each group are shown in Fig. 2(a) and 2(c), respectively. Most of the regions identified in this process belong to the default mode areas that are well known to be active during resting condition (Greicius et al., 2003; Raichle et al., 2001). A more interesting ranking process is the ranking of regions affected during OCD. This information is captured using the *differential node entropy* of nodes. The regions extracted using this procedure (Algorithm 1) are illustrated in two ways - (1) visualizing the nodes corresponding to highly ranked regions as shown in Fig. 2(b), and (2) listing the top-25 regions in Table 3. Furthermore, the corresponding *differential entropy* value and *p*-value for each region's node entropy are also shown in the same Table. There are 13 regions with statistically significant difference ($p < 0.05$) in node entropy among the 25 regions.

Note that the ranking can be validated for OCD by considering the regions from CSTC circuitry (Bernstein et al., 2016). Our ranking methodology is able to capture the regions from that circuit in top 15% of these most important nodes. We illustrate the differential node entropy values for the regions in sorted order in Fig. S3 (SI). In addition, we also show the mean *differential entropy* value and standard deviation

(SD) in the same figure. There are 13 regions with *differential entropy* more than 1-SD away from mean. Also, 38 regions have differential entropy values more than mean. Another ranking scheme using 2-hop neighbors (here neighborhood for a node is defined based on distance of 2 edges from a node) revealed the most important regions to be similar to 1-hop neighbors (Table S1 in SI). The leave-one-out classification performance using all node entropy values is shown in Table 2 and is 0.71.

3.3.3. Ranking of edges

The most important ranked edges are visualized by overlaying them on an MNI brain using BrainNet toolbox (Xia et al., 2013) (Fig. 3). The group ranking procedure based on edge entropy (Eq. (7) and Algorithm S2 in SI) extracts top edges from healthy, and OCD separately as shown in Fig. 3(a) and (c), respectively. Top 100 edges were identified using the ranking process for each group. Additionally, the ranking based on *differential edge entropy* is also visualized in Fig. 3(b). A close inspection of the results reveals several observations. First, for each group ranking procedure reveals edges that are distributed throughout the lateral and medial cortical part of the brain and some of them belong to the default mode network. Second, *differential entropy* elevates the edges that belong to fronto-parietal and frontal-subcortical areas. The regions that are connected using the edges belong to frontal lobe, parietal lobe, anterior and posterior cingulate gyrus, thalamus proper, default mode (DMN), accumbens (striatal area) and amygdala. The corresponding differential entropy values for the edges are shown in sorted order in Fig. S4 (SI).

3.4. Extracting predictive sub-network

3.4.1. Accuracy of predictive sub-network

Following the method as outlined in Fig. 1, we ran our edge ranking procedure Algorithm 1 for edges 28 times, each time selecting top edges for leave-one-out classification. The change in classification accuracy with the number of edges using SVM and radial basis function kernel (using only selected edges) is shown in Fig. 4. The classification accuracy has a behavior similar to traditional feature selection algorithms where it improves up to 120 edges and then starts to decrease. In order to understand the significance of the current work with the information about sub-network, the result is compared with a number of baseline network based features in terms of classification accuracy. The comparisons of leave-one-out classification results are shown in Table 2. In addition, results for repeated random sub-sampling validation (cross-validation process run 100 times, each time randomly splitting the
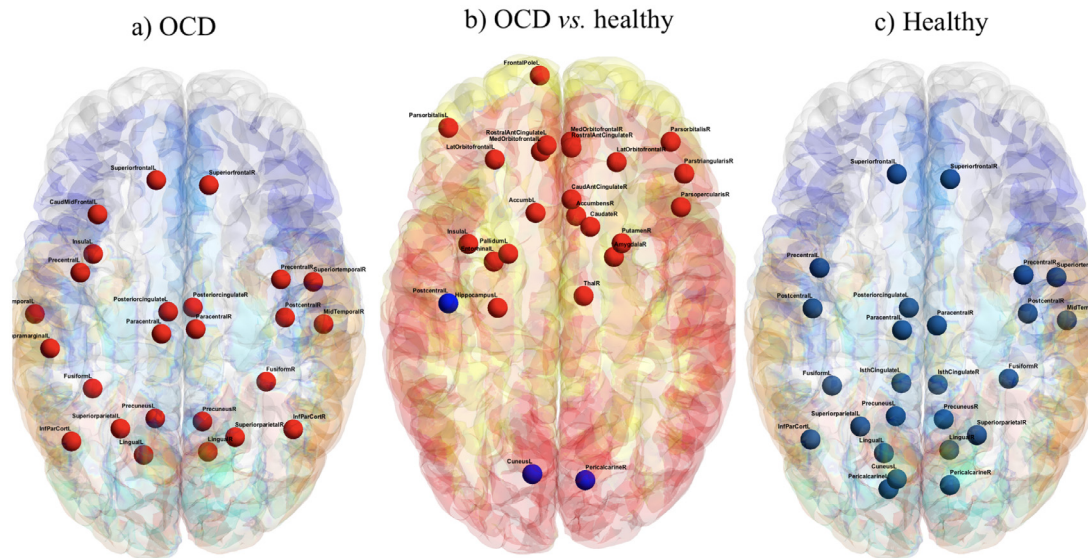
Fig. 2. Visualization of important regions that have differences in entropy between OCD and healthy groups corresponding to frequency band B1 at network sparsity 35%. (a) OCD, *red:* regions that have higher entropy. (b) Differentiating regions between OCD *vs.* healthy, *red:* regions that have higher entropy for OCD, *blue:* regions that have higher entropy for healthy. (c) Healthy *blue:* regions that have higher entropy for healthy. (For interpretation of the references to color in this figure legend, the reader is referred to the web version of this article.)

Table 3
Top-25 regions extracted using *differential node entropy* for OCD *vs.* healthy controls.

Rank	Region/Hemisphere	Diff. Entropy	*p*-value
1	Parsopercularis - R	1.5099	**0.0002**
2	Thalamus Proper - R	0.9660	**0.0129**
3	Parsorbitalis - L	0.9252	**0.0459**
4	Cuneus - L	0.9098	**0.0153**
5	Accumbens Area - L	0.9095	**0.0159**
6	Postcentral - L	0.9021	**0.0065**
7	Parsorbitalis - R	0.8944	**0.0427**
8	Pallidum - L	0.8514	0.0944
9	Medial Orbitofrontal - L	0.8303	**0.0476**
10	Parstriangularis - R	0.8233	**0.0500**
11	Medial Orbitofrontal - R	0.8090	**0.0392**
12	Amygdala - R	0.7317	0.1534
13	Hippocampus - L	0.7103	0.1503
14	Lateral Orbitofrontal - L	0.6737	0.1846
15	Caudate - R	0.6620	**0.0234**
16	Rostral Anterior Cingulate - R	0.6574	0.1239
17	Rostral Anterior Cingulate - L	0.6378	0.1657
18	Lateral Orbitofrontal - R	0.6201	0.2251
19	Pericalcarine - R	0.6192	**0.0188**
20	Caudal Anterior Cingulate - R	0.6165	0.2049
21	Entorhinal - L	0.6147	0.1431
22	Frontal Pole - L	0.5782	0.2752
23	Insula - L	0.5692	0.1392
24	Putamen - R	0.5565	**0.0318**
25	Accumbens Area - R	0.5419	0.1184

dataset into training 23 subjects and testing 5 subjects) are shown in Supplementary Information Table S3. Edge entropies of the proposed predictive sub-network achieved 0.89 accuracy and correctly classify all healthy and 12 out of 15 OCD subjects. Using 2-hop neighbor scheme for classification did not improve the accuracy (see Table S2 in SI). In our study, SVM was chosen based on the performance of multiple classifiers (e.g., support vector machine, linear discriminant analysis, artificial neural network and random forest). Their comparison of performance is shown in Supplementary Information Table S4.

3.4.2. Sub-network visualization

The identified sub-network comprising 33 region and 120 edges is shown in Fig. 5. In Table S5 (SI), we list the regions from predictive sub-

network as well as well as the CSTC network. Top-50 edges from the sub-network are also listed in Table S6 (SI). In both cases, whether the regions or edges belong to CSTC network are also illustrated.

3.4.3. Statistical analysis

We selected the top-120 features in each iteration for leave-one-out training, and plot their occurrence using a histogram as shown in Fig. S5 in SI. The top ranked edges shown in Fig. 5 are also very important for classification as they are selected most of the times as top edges. In addition, the predictive sub-network achieves a *p*-value of 0.0071 for a *t*-test of *sub-graph* entropies between OCD *vs.* healthy as demonstrated in Table 4. Similarly, CSTC sub-graph entropy is significantly reduced ($p = 0.0077$) for OCD. The box plot for the *t*-test is shown in Fig. 6. To validate that the classifier performs significantly better than chance, permutation tests were performed, the results of which are shown in Fig. 7.

4. Discussion

This paper investigates the feasibility of automated classification of adolescent OCD *vs.* matched healthy controls. It proposes the use of *information-theoretic sub-graph* entropy for ranking regions and edges from a group of brain scans and extracting a predictive sub-network for differentiating adolescent OCD patients from healthy. The predictive frequency band was found to be B1 (low frequency BOLD oscillation) at network sparsity level 35%. Key observations from different classification approaches are discussed in this section.

4.1. Regions and edges

The present findings advance the method of resting-state fMRI analysis to examine neural networks in youth with OCD by network analysis; all prior methods had used standard, traditional approaches to examining functional connectivity (Bernstein et al., 2016; Fitzgerald et al., 2011; 2011; Gruner et al., 2016; Weber et al., 2014). Fitzgerald et al. (2011) have found lower functional network connectivity in the cortico-striato-thalamo-cortical circuitry for youth OCD subjects in the age range 8–12. Fitzgerald et al. (2011) also reported decreased amount of functional connections in the anterior cingulate cortex, striatal and thalamus areas. Gruner et al. (2016) and
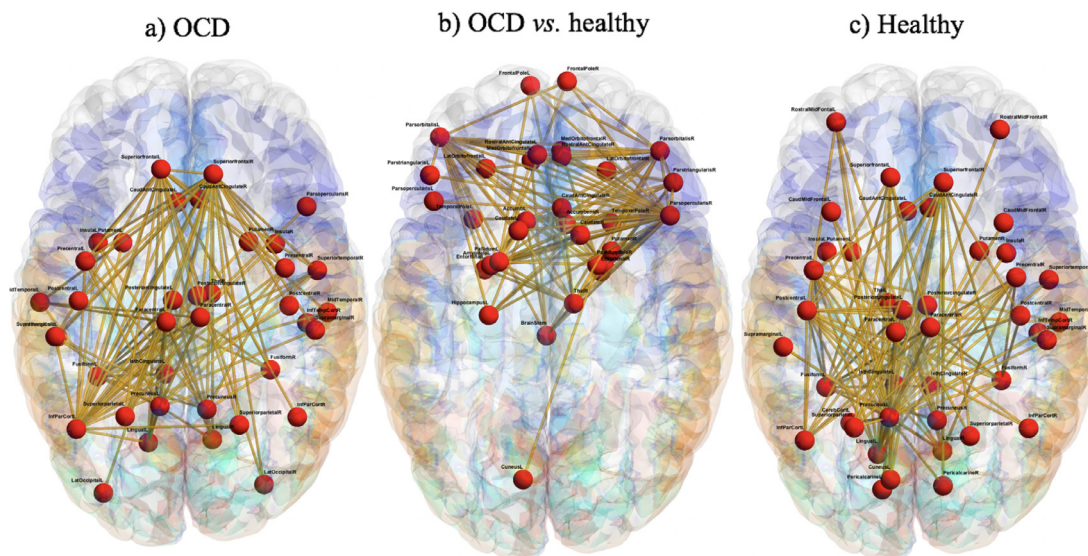
Fig. 3. Visualization of important edges that have differences in entropy between OCD and healthy groups corresponding to frequency band B1 at network sparsity 35%. (a) OCD, (b) Differentiating edges between OCD *vs.* healthy. (c) Healthy.
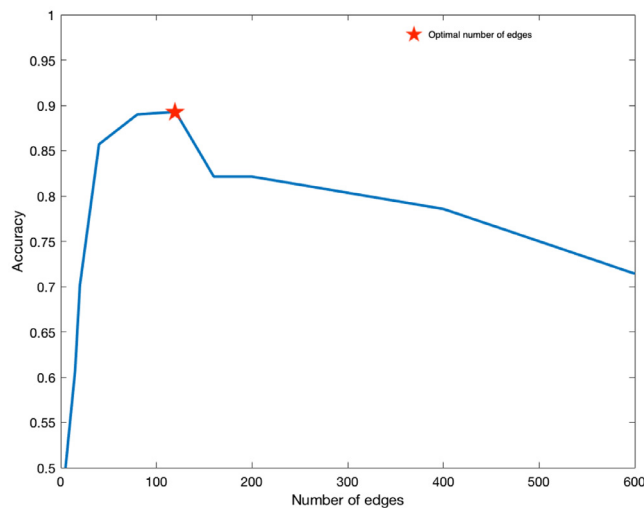

Fig. 4. Average Leave-one-out accuracy *vs.* number of edges in sub-network.

Weber et al. (2014) used independent component analysis (ICA), a multivariate blind source separation technique, to analyze whole brain functional network of adolescent OCD subjects. Functional connectivity scores corresponding to each component were observed to be significantly higher among OCD patients in comparison with matched healthy controls in anterior/ posterior cingulate cortical areas and significantly sparser in visual cortical areas. Weber et al. (2014) also reported reduced functional connections in the cingulate cortex. Bernstein et al. (2016) found decreased connectivity between putamen and lateral prefrontal cortex. Also, Bernstein et al. (2016) found lower connectivity between the putamen and the right insula and operculum.

Using the methods described here, we were able to capture previously known regions for resting-state fMRI scans from healthy humans (Greicius et al., 2008). Notably, all of the top-ranked regions that were identified to have high node entropy values for each group are default mode network nodes associated with resting-state. In addition, the OCD group showed higher regional entropy for regions such as thalamus, hippocampus, accumbens, putamen, anterior cingulate, postcentral gyrus, amygdala, pars-orbitalis and pars-opercularis as shown in Fig. 2. Interestingly, the high ranking of the thalamus and hippocampus regions by the proposed differential entropy approach is

consistent with the traditional hypothesis that these regions are affected for subjects suffering from OCD. The regions and edges that had most difference between healthy *vs.* OCD consist of accumbens, amygdala, thalamus, pallidum which are part of the CSTC circuit (Bernstein et al., 2016) in brain. This circuit is shown in Fig. S6 in Supplementary Information. The intersection between CSTC and predictive sub-network is also illustrated in Fig. S7 (SI).

In Figs. 3 and 5, we show the top ranked predictive edges between important brain nodes for two groups (OCD *vs.* controls). The predictive network consists of many regions that act as hub (Bullmore and Sporns, 2009), *i.e.*, they consist of a number of edges that differentiated OCD group from healthy controls. Some of the edges include connection from operculum to putamen, accumbens, thalamus. Furthermore, edges from frontal pole to striatal regions also form a substantial part of the predictive network. The edge between amygdala and occipital lobe (cuneus) also distinguished OCD patients and healthy, which is notable as it represents a connection linking the default mode network and the limbic network. Edges that are not common between CSTC and predictive network are shown in Fig. S8 and S9, respectively. These plots illustrate how the proposed sub-network differs from the CSTC network. While the use of the edge entropies of the CSTC sub-network achieved an accuracy of 0.71, that of the proposed sub-network led to an accuracy of 0.89. This emphasizes the importance of including whole-brain data in the analysis, rather than focusing on just the CSTC. Although classifying OCD with high accuracy has been known to be difficult, the proposed sub-network improves the achievable accuracy significantly compared to all prior approaches.

At a group level, the top discriminating links between OCD *vs.* controls are also statistically significant ($p < 0.05$). The individual edge entropy measures are useful metrics for classification as the proposed classifier significantly outperforms the classification with Pearson correlation coefficient values. However, the *sub-graph entropy* has significant reduction for OCD patients for both CSTC network and predictive sub-network as shown in Fig. 6.

Fig. 2 shows a number of nodes that differentiated OCD versus controls, and they are mostly *red*, signifying that they had higher entropy in OCD than controls. However Fig. 6 shows that for both the CSTC network and the predictive network *sub-graph* entropy is lower. Although the nodes in OCD subjects tend to have higher node entropy, the *sub-graphs* used to calculate the node entropy consider only the neighbors the node is connected with. The predictive *sub-graph* is a different *sub-graph* that is extracted considering the most predictive
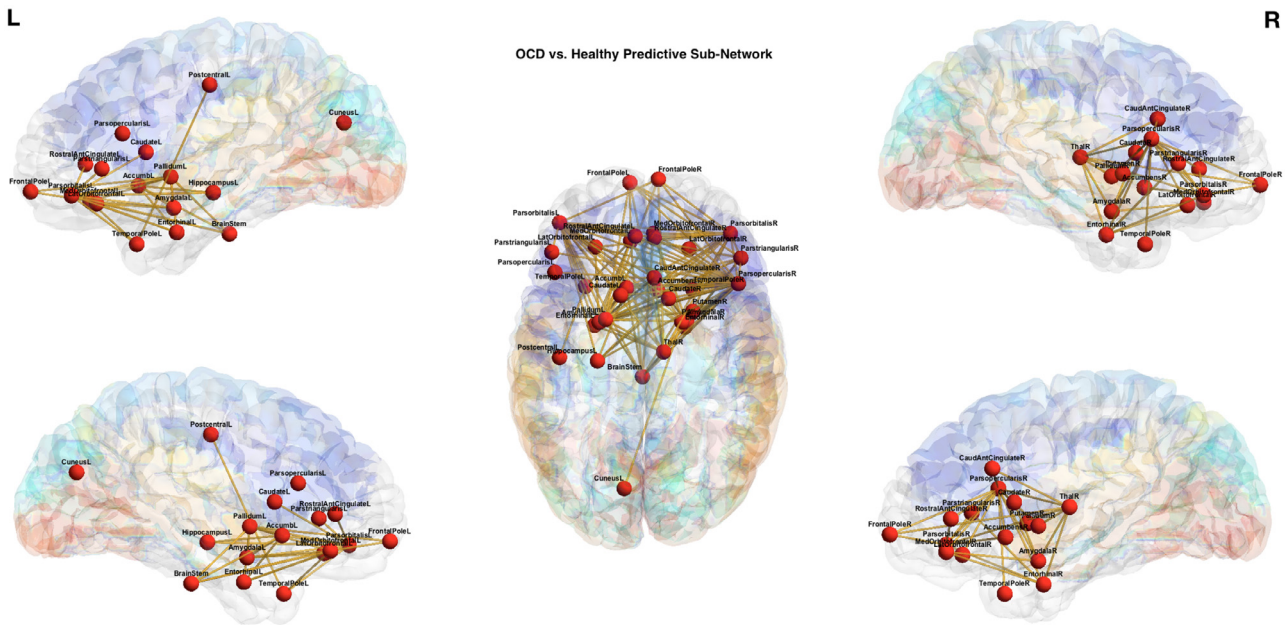
Fig. 5. Predictive sub-network extracted using *differential edge entropy* and leave-one-out analysis. This network corresponds to frequency band B1 and density threshold of 35%.

edges based on edge entropy. The apparent difference in these two indicate that, although the nodes (that might be part of predictive sub-network) may have higher node entropy, the overlap of the edges (containing the nodes) that belong to the predictive sub-network is lower. In addition, this also indicates that the edge weights (in the predictive sub-network) are relatively well distributed in healthy controls (that lead to higher *sub-graph* entropy), and skewed in OCD patients (the lead to low *sub-graph* entropy).

4.2. Misclassified subjects

The OCD severity (CY-BOCS) of the patient group varied between 12–27. The mean, standard deviation and median were 19.7, 3.5, and 20, respectively. The OCD severity of misclassified subjects were 12, 15 and 19, respectively. Two of the misclassified subjects were under medication and one was non-medicated. The misclassified subjects fall in the lower end of CY-BOCS for the group of subjects. The inability of the classifier to distinguish these patients may indicate that these subjects had relatively mild level of OCD symptoms as indicated by their CY-BOCS score. The classifier identified them to fall in healthy group. A histogram illustrating the OCD severity of subjects and the CY-BOCS score for misclassified subjects is shown in Supplementary Information Fig. S10.

4.3. Validation

The binomial test on the classification using the proposed sub-network also shows that they have statistically significant predictive performance ($p = 7.9497 \times 10^{-06}$ for OCD *vs.* healthy with respect to a naive classifier and $p = 0.0009$ with respect to Sen et al. (2016)). In

order to further validate the *information-theoretic* model, a sub-network containing only regions from CSTC circuits is extracted as shown in Fig. S6 and the *sub-graph* entropy between patient *vs.* control group is compared as shown in Fig. 6. CSTC *sub-graph* entropy is significantly reduced ($p = 0.0077$, as illustrated in Table 4) for OCD. In order to avoid potential problem with overfitting, leave-one-out classification with in-fold feature selection was used in every experimental setting. Note that this makes sure that the classifier is learning features from the training set and using the learned feature for finding the test accuracy in order to generalize the diagnosis to previously unseen subject.

Although the classification used in this paper is leave-one-out, the result is robust even in the case of 5-fold cross validation and repeated random sub-sampling validation. For 5-fold CV, the dataset was divided into 5 sets each consisting of 5, 5, 6, 6, 6 subjects (5-folds), respectively. In each fold, one set was used for testing and others for training. We found out that edge entropy with 120 features achieve the same accuracy, specificity and sensitivity as leave-one-out. For repeated random sub-sampling validation, the cross-validation process was run 100 times, each time randomly splitting the dataset into training (23 subjects) and testing (5 subjects). The results for this procedure for each types of features are shown in Supplementary Information Table S3. Edge sub-network and Union sub-graph achieved accuracy of 0.87, specificity of 0.96 and sensitivity of 0.79. All these values are within 4% of leave-one-out accuracy and better than the performance of other features.

In order to reinforce our conclusion that the classification performance of the extracted predictive network from the model are better than baseline models, permutation tests were performed. In this vein, a 'naive' baseline model was created effectively by permuting the labels in the training and test set. Thus the baseline model removed all the

Table 4
Statistical analysis of predictive sub-network and CSTC network using *sub-graph* entropy.

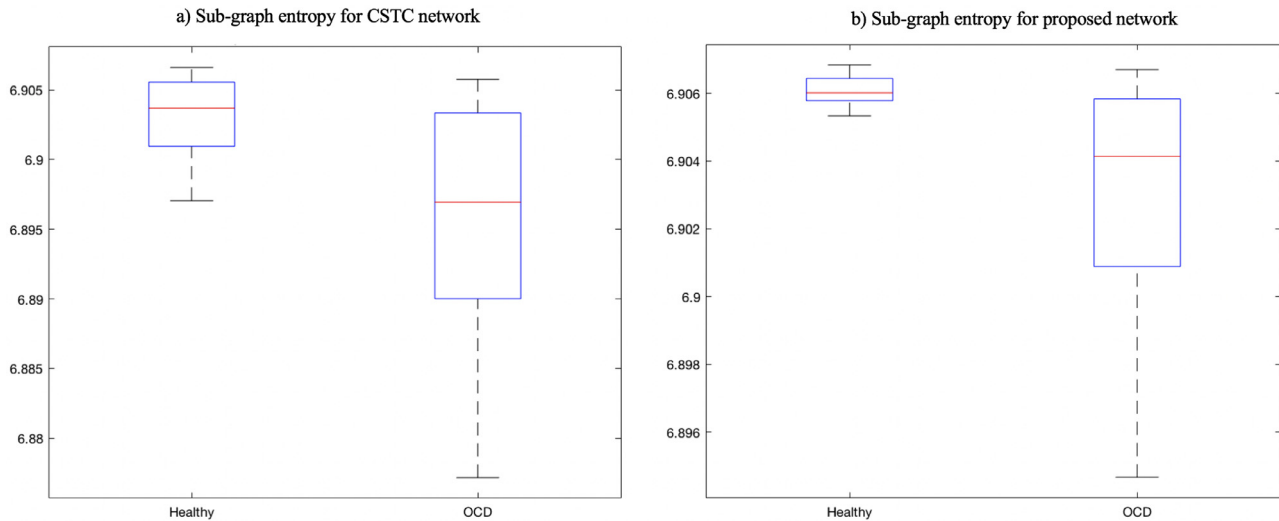|	# of nodes	# of edges	Sub-graph entropy		p-value
			Mean	SD	
Proposed sub-network	33	120	Healthy: 6.9061 OCD: 6.9028	Healthy: 0.0004 OCD: 0.0039	**0.0071**
CSTC sub-network	16	120	Healthy: 6.9030 OCD: 6.8951	Healthy: 0.0032 OCD: 0.0090	**0.0077**

Fig. 6. Box-plot of *sub-graph entropy* values for OCD *vs*. healthy, (a) CSTC sub-network, (b) predictive sub-network.
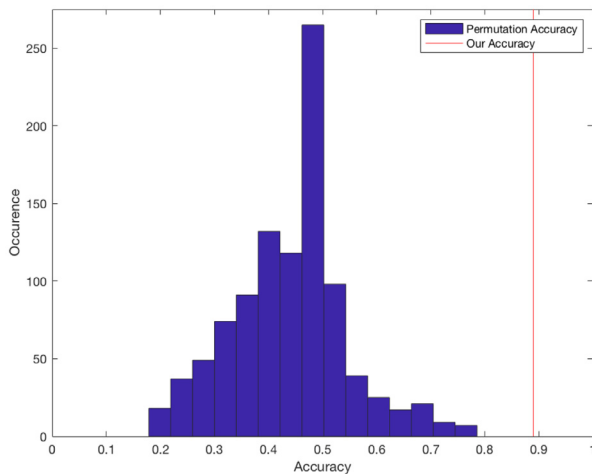

Fig. 7. Results of permutation test on OCD data. The labels for healthy and OCD are permuted and a SVM classifier is fitted to each new dataset. Histogram of accuracies and accuracy on actual data is shown.

signals associated with OCD from the labels - the leave-one-out classifier then learned the relationships between the edge entropy and permuted labels. The actual learned model performed significantly better than baseline which suggests that the classification scheme outlined before is also statistically significant. Here, for OCD *vs*. healthy dataset, 1000 iterations were performed where each time, labels were permuted and then trained using an SVM model on the training subset of this set and tested on the rest. Fig. 7 shows the distributions of accuracy values for the dataset. In this scenario, there is a significant distance between the centre of the accuracy distribution and the accuracy produced by the predictive sub-network.

4.4. Predictive sub-network as part of other known networks

Our results implicate regions and edges from a number of large-scale brain networks. Here we discuss potential interpretations for the involvement of these networks in adolescent OCD.

4.4.1. Default mode network (DMN)
The default mode network of human brain consists of regions that are active when a person is awake but resting and not doing any particular task (Biswal et al., 1995; Greicius et al., 2003). The DMN regions are typically associated with mind wandering, day dreaming, thoughts

about the self, and ruminations etc. In our analysis, the top regions, edges and predictive network extracted using *sub-graph* entropy consist of regions from the DMN. This may indicate that adolescents suffering from OCD can get "stuck" in repetitive thought patterns. Previous works also support the hypothesis that OCD involves abnormalities of the DMN (Beucke et al., 2014; Hou et al., 2013; Stern et al., 2012).

4.4.2. Dorsal attention + salience
The dorsal attention network contains regions that show increased activation when a subject is deciding where to focus the attention in a proactive way. The salience network provides the mechanism to attend the important cues that stand out compared to the background. In our results, the predictive sub-network contains regions (entorhinal) from dorsal attention (Bell and Shine, 2015; Yuan et al., 2016) network. Moreover, it contains the hippocampus which is part of salience network (Bressler and Menon, 2010; Heine et al., 2012; Riedl et al., 2016; Yeo et al., 2011). The functional regions and edges containing salience and dorsal attention indicate that OCD subjects may deploy attention and attending visual cues differently from healthy adolescents (Chen et al., 2018; Fasching et al., 2016; Nestadt et al., 2016).

4.4.3. Executive network
The executive network, which consists of fronto-parietal brain regions, is responsible for high level cognition functions, such as, problem solving, and decision-making. The predictive sub-network implicated for adolescent OCD includes many regions from frontal part of the brain (Fig. 1), *e.g.*, orbitofrontal, fontal pole, parsorbitalis, and also parietal part of brain, *e.g.*, postcentral gyrus. Their involvement in prediction performance may indicate the change in executive functions in OCD patients compared with healthy subjects (Bannon et al., 2006; Kashyap et al., 2013; Stern et al., 2012).

4.4.4. Limbic network
Finally, the predictive sub-network contains the following regions from limbic system - hippocampus and amygdala. Limbic regions play a critical role in mediating emotional responses and forming new memories. This functional network has been shown to be affected for OCD patients in a number of previous studies (Modell et al., 1989; Saxena and Rauch, 2000; Sheth et al., 2013). Specifically, amygdala had higher node entropy value compared with controls, which may indicate its utility for relieving the elevated anxiety level for OCD patients.

5. Conclusion and future work

Using an *information-theoretic* network approach, this paper has identified a predictive sub-network of the brain that can be used to discriminate brain networks of adolescents with OCD from healthy controls. The regions and edges that are found to be most important based on *differential entropy* are also found to be statistically significant. The predictive sub-network contains brain regions from well known large-scale brain functional networks. Their involvement implies possible impairment of brain function of adolescents suffering from OCD. However, one limitation of the current work is the small number of participants in each group. Therefore, future work needs to be directed towards analysis of datasets with larger sample size. In addition, features and classifier models need to be developed to predict the onset of OCD and other psychiatric disorders like depression. Future work may also be directed towards classification based on frequency-domain features.

6. Declaration of Competing Interest

The authors declare no competing financial interests.

Supplementary material

Supplementary material associated with this article can be found, in the online version, at 10.1016/j.nicl.2020.102208 .

References

Armañanzas, R., Iglesias, M., Morales, D.A., Alonso-Nanclares, L., 2016. Voxel-based diagnosis of Alzheimer's disease using classifier ensembles. IEEE J. Biomed. Health Inform. 21 (3), 778–784.

Armstrong, C.C., Moody, T.D., Feusner, J.D., McCracken, J.T., Chang, S., Levitt, J.G., Piacentini, J.C., ONeill, J., 2016. Graph-theoretical analysis of resting-state fMRI in pediatric obsessive–compulsive disorder. J. Affect. Disord. 193, 175–184.

Atluri, G., MacDonald III, A., Lim, K.O., Kumar, V., 2016. The brain-network paradigm: using functional imaging data to study how the brain works. Computer 49 (10), 65–71.

Bannon, S., Gonsalvez, C.J., Croft, R.J., Boyce, P.M., 2006. Executive functions in obsessive–compulsive disorder: state or trait deficits? Aust. N.Z. J. Psychiatry 40 (11–12), 1031–1038.

Bao, T., Klatt, B.N., Whitney, S.L., Sienko, K.H., Wiens, J., 2019. Automatically evaluating balance: a machine learning approach. IEEE Trans. Neural Syst. Rehabil. Eng. 27 (2), 179–186.

Bassett, D.S., Nelson, B.G., Mueller, B.A., Camchong, J., Lim, K.O., 2012. Altered resting state complexity in schizophrenia. Neuroimage 59 (3), 2196–2207.

Bell, P.T., Shine, J.M., 2015. Estimating large-scale network convergence in the human functional connectome. Brain Connect. 5 (9), 565–574.

Bernstein, G., Mueller, B., Schreiner, M.W., Campbell, S.M., Regan, E.K., Nelson, P.M., Houri, A.K., Lee, S.S., Zagoloff, A.D., Lim, K.O., Yacoub, E.S., Cullen, K.R., 2016. Abnormal striatal resting-state functional connectivity in adolescents with obsessive–compulsive disorder. Psychiatry Res. 247, 49–56.

Bernstein, G.A., Victor, A.M., Nelson, P.M., Lee, S.S., 2013. Pediatric obsessive–compulsive disorder: symptom patterns and confirmatory factor analysis. J. Obsess. Compuls. Relat. Disord. 2 (3), 299–305.

Beucke, J.C., Sepulcre, J., et al., 2014. Default mode network subsystem alterations in obsessive–compulsive disorder. Br. J. Psychiatry 205 (5), 376–382.

Biswal, B., Zerrin Yetkin, F., Haughton, V.M., Hyde, J.S., 1995. Functional connectivity in the motor cortex of resting human brain using echo-planar MRI. Magn. Reson. Med. 34 (4), 537–541.

Bressler, S.L., Menon, V., 2010. Large-scale brain networks in cognition: emerging methods and principles. Trends Cogn. Sci. 14 (6), 277–290.

Bullmore, E., Sporns, O., 2009. Complex brain networks: graph theoretical analysis of structural and functional systems. Nat. Rev. Neurosci. 10 (3).

Chen, Y.-H., Li, S.-F., Lv, D., Zhu, G.-D., Wang, Y.-H., Meng, X., Hu, Q., Li, C.-C., Zhang, L.-T., Chu, X.-P., et al., 2018. Decreased intrinsic functional connectivity of the salience network in drug-naive patients with obsessive-compulsive disorder. Front. Neurosci. 12, 889.

Coifman, R.R., Wickerhauser, M.V., 1992. Entropy-based algorithms for best basis selection. IEEE Trans. Inf. Theory 38 (2), 713–718.

Desikan, R.S., Ségonne, F., et al., 2006. An automated labeling system for subdividing the human cerebral cortex on MRI scans into gyral based regions of interest. Neuroimage 31 (3), 968–980.

Donoho, D.L., Johnstone, I.M., et al., 1994. Ideal denoising in an orthonormal basis chosen from a library of bases. Compt. Rend. L'Acad. Sci. 319 (12), 1317–1322.

Dragomir, A., Vrahatis, A.G., Bezerianos, A., 2018. A network-based perspective in alzheimer's disease: current state and an integrative framework. IEEE J. Biomed. Health Inform. 23 (1), 14–25.

Fasching, J., Walczak, N., Bernstein, G.A., et al., 2016. Automated coding of activity videos from an OCD study. 2016 IEEE International Conference on Robotics and Automation (ICRA). IEEE, pp. 5638–5643.

Feinberg, D.A., Moeller, S., Smith, S.M., Auerbach, E., Ramanna, S., Glasser, M.F., Miller, K.L., Ugurbil, K., Yacoub, E., 2010. Multiplexed echo planar imaging for sub-second whole brain fMRI and fast diffusion imaging. PLoS ONE 5 (12), e15710.

Fitzgerald, K.D., Welsh, R.C., Stern, E.R., Angstadt, M., Hanna, G.L., Abelson, J.L., Taylor, S.F., 2011. Developmental alterations of frontal-striatal-thalamic connectivity in obsessive-compulsive disorder. J. Am. Acad. Child Adolesc. Psychiatry 50 (9), 938–948.

Freeman, L.C., Roeder, D., Mulholland, R.R., 1979. Centrality in social networks: II. Experimental results. Soc. Netw. 2 (2), 119–141.

Grabill, K., Merlo, L., Duke, D., Harford, K.L., Keeley, M.L., Geffken, G.R., Storch, E.A., 2008. Assessment of obsessive–compulsive disorder: a review. J. Anxiety Disord. 22 (1), 1–17.

Greicius, M.D., Krasnow, B., Reiss, A.L., Menon, V., 2003. Functional connectivity in the resting brain: a network analysis of the default mode hypothesis. Proc. Natl. Acad. Sci. 100 (1), 253–258.

Greicius, M.D., Supekar, K., Menon, V., Dougherty, R.F., 2008. Resting-state functional connectivity reflects structural connectivity in the default mode network. Cereb. Cortex 19 (1), 72–78.

Gruner, P., Anticevic, A., Lee, D., Pittenger, C., 2016. Arbitration between action strategies in obsessive-compulsive disorder. Neurosci. 22 (2), 188–198.

Heine, L., Soddu, A., Gómez, F., Vanhaudenhuyse, A., Tshibanda, L., Thonnard, M., Charland-Verville, V., Kirsch, M., Laureys, S., Demertzi, A., 2012. Resting state networks and consciousness. Front. Psychol. 3, 295.

Hou, J., Song, L., Zhang, W., Wu, et al., 2013. Morphologic and functional connectivity alterations of corticostriatal and default mode network in treatment-naïve patients with obsessive-compulsive disorder. PLoS ONE 8 (12), e83931.

Huang, J., Zhu, Q., Hao, X., Shi, X., Gao, S., Xu, X., Zhang, D., 2018. Identifying resting-state multifrequency biomarkers via tree-guided group sparse learning for schizophrenia classification. IEEE J. Biomed. Health Inform. 23 (1), 342–350.

Jenkinson, M., Beckmann, C.F., Behrens, T.E.J., Woolrich, M.W., Smith, S.M., 2012. FSL. Neuroimage 62 (2), 782–790.

Kashyap, H., Kumar, J.K., Kandavel, T., Reddy, Y., 2013. Neuropsychological functioning in obsessive-compulsive disorder: are executive functions the key deficit? Compr. Psychiatry 54 (5), 533–540.

King, R., Leonard, H., March, J., 1998. Practice parameters for the assessment and treatment of children and adolescents with obsessive compulsive disorder. J. Am. Acad. Child Adolesc. Psychiatry 10 (suppl), 37.

Körner, J., 1973. Coding of an information source having ambiguous alphabet and the entropy of graphs. 6th Prague Conference on Information Theory. pp. 411–425.

Latora, V., Marchiori, M., 2001. Efficient behavior of small-world networks. Phys. Rev. Lett. 87 (19), 198701.

Li, A., Pan, Y., 2016. Structural information and dynamical complexity of networks. IEEE Trans. Inf. Theory 62 (6), 3290–3339.

Lynall, M., Bassett, D., Kerwin, R., McKenna, P.J., Kitzbichler, M., Muller, U., Bullmore, E., 2010. Functional connectivity and brain networks in schizophrenia. J. Neurosci. 30 (28), 9477–9487.

Mackenzie, K.D., 1966. The information theoretic entropy function as a total expected participation index for communication network experiments. Psychometrika 31 (2), 249–254.

Mitterschiffthaler, M.T., Ettinger, U., Mehta, M.A., Mataix-Cols, D., Williams, S.C., 2006. Applications of functional magnetic resonance imaging in psychiatry. J. Mag. Reson. Imaging 23 (6), 851–861.

Modell, J.G., Mountz, J.M., Curtis, G.C., Greden, J.F., 1989. Neurophysiologic dysfunction in basal ganglia/limbic striatal and thalamocortical circuits as a pathogenetic mechanism of obsessive-compulsive disorder. J. Neuropsychiatry Clin. Neurosci.

Nestadt, G., Kamath, V., Maher, B.S., Others, 2016. Doubt and the decision-making process in obsessive-compulsive disorder. Med. Hypotheses 96, 1–4.

Newman, M.E.J., 2006. Modularity and community structure in networks. Proc. Nat. Acad. Sci. 103 (23), 8577–8582.

Peng, H., Long, F., Ding, C., 2005. Feature selection based on mutual information: criteria of max-dependency, max-relevance, and min-redundancy. IEEE Trans. Pattern Anal. Mach.Intell. (8), 1226–1238.

Raichle, M.E., MacLeod, A.M., Snyder, A.Z., Powers, W.J., Gusnard, D.A., Shulman, G.L., 2001. A default mode of brain function. Proc. Nat. Acad. Sci. 98 (2), 676–682.

Rasmussen, S.A., Eisen, J.L., 1992. The epidemiology and differential diagnosis of obsessive-compulsive disorder. Zwangsstörungen/Obsessive-Compulsive Disorders. Springer, pp. 1–14.

Richiardi, J., Achard, S., Bunke, H., Van De Ville, D., 2013. Machine learning with brain graphs: predictive modeling approaches for functional imaging in systems neuroscience. IEEE Signal Process. Mag. 30 (3), 58–70.

Riedl, V., Utz, L., Castrillón, G., Grimmer, T., Rauschecker, J.P., Ploner, M., Friston, K.J., Drzezga, A., Sorg, C., 2016. Metabolic connectivity mapping reveals effective connectivity in the resting human brain. Proc. Natl. Acad. Sci. 113 (2), 428–433.

Rosario-Campos, M., Miguel, E., Quatrano, S., Chacon, P., Ferrao, Y., Findley, D., Katsovich, L., Scahill, L., King, R., Woody, S., et al., 2006. The dimensional yale–brown obsessive–compulsive scale (dy-bocs): an instrument for assessing obsessive–compulsive symptom dimensions. Mol. Psychiatry 11 (5), 495.

Rosso, O.A., Blanco, S., Yordanova, J., Kolev, V., Figliola, A., Schürmann, M., Başar, E., 2001. Wavelet entropy: a new tool for analysis of short duration brain electrical signals. J. Neurosci. Methods 105 (1), 65–75.

Rubinov, M., Sporns, O., 2010. Complex network measures of brain connectivity: uses and interpretations. Neuroimage 52 (3), 1059–1069.

Saxena, S., Rauch, S.L., 2000. Functional neuroimaging and the neuroanatomy of obsessive-compulsive disorder. Psychiatric Clin. North Am. 23 (3), 563–586.

Sen, B., Bernstein, G.A., Xu, T., Mueller, B.A., Schreiner, M.W., Cullen, K.R., Parhi, K.K., 2016. Classification of obsessive-compulsive disorder from resting-state fMRI. IEEE 38th Annual International Conference of the Engineering in Medicine and Biology Society (EMBC). pp. 3606–3609.

Sen, B., Chu, S.-H., Parhi, K.K., 2019. Ranking regions, edges and classifying tasks in functional brain graphs by sub-graph entropy. Sci. Rep. 9 (1), 7628.

Sen, B., Mueller, B., Klimes-Dougan, B., Cullen, K., Parhi, K.K., 2019. Classification of major depressive disorder from resting-state fMRI. 2019 41st Annual International Conference of the IEEE Engineering in Medicine and Biology Society (EMBC). pp. 3511–3514. https://doi.org/10.1109/EMBC.2019.8856453.

Sen, B., Parhi, K.K., 2017. Extraction of common task signals and spatial maps from group fMRI using a parafac-based tensor decomposition technique. 2017 IEEE International Conference on Acoustics, Speech and Signal Processing (ICASSP). IEEE, pp. 1113–1117.

Sheth, S.A., Neal, J., Tangherlini, F., Mian, M.K., Gentil, A., Cosgrove, G.R., Eskandar, E.N., Dougherty, D.D., 2013. Limbic system surgery for treatment-refractory obsessive-compulsive disorder: a prospective long-term follow-up of 64 patients. J. Neurosurg. 118 (3), 491–497.

Sporns, O., 2003. Graph theory methods for the analysis of neural connectivity patterns.

Neuroscience Databases. Springer, pp. 171–185.

Stern, E.R., Fitzgerald, K.D., Welsh, R.C., Abelson, J.L., Taylor, S.F., 2012. Resting-state functional connectivity between fronto-parietal and default mode networks in obsessive-compulsive disorder. PLoS ONE 7 (5), e36356.

Weber, A.M., Soreni, N., Noseworthy, M.D., 2014. A preliminary study of functional connectivity of medication naive children with obsessive–compulsive disorder. Prog. Neuro-Psychopharmacol. Biol. Psychiatry 53, 129–136.

Xia, M., Wang, J., He, Y., 2013. Brainnet viewer: a network visualization tool for human brain connectomics. PLoS ONE 8 (7), e68910.

Xu, T., Cullen, K.R., Mueller, B., Schreiner, M.W., Lim, K.O., Schulz, S.C., Parhi, K.K., 2016. Network analysis of functional brain connectivity in borderline personality disorder using resting-state fMRI. NeuroImage 11, 302–315.

Yeo, B.T., Krienen, F.M., Sepulcre, J., et al., 2011. The organization of the human cerebral cortex estimated by intrinsic functional connectivity. J. Neurophysiol. 106 (3), 1125–1165.

Yuan, R., Di, X., Taylor, P.A., Gohel, S., Tsai, Y.-H., Biswal, B., 2016. Functional topography of the thalamocortical system in human. Brain Struct. Funct. 221 (4), 1971–1984.

Zalesky, A., Fornito, A., Bullmore, E.T., 2010. Network-based statistic: identifying differences in brain networks. Neuroimage 53 (4), 1197–1207.